Korean J. Chem. Eng., 38(6), 1224-1230 (2021)
DOI: 10.1007/s11814-021-0758-8

pISSN: 0256-1115
eISSN: 1975-7220

Methane oxidation to formaldehyde over vanadium oxide supported on various mesoporous silicas

Euiseob Yang*, Jun Gyeong Lee*, Eun Duck Park,†, and Kwangjin An*,†**

*School of Energy and Chemical Engineering, Ulsan National Institute of Science and Technology (UNIST), Ulsan 44919, Korea
**Department of Chemical Engineering and Department of Energy Systems Research, Ajou University, Suwon 16499, Korea
(*Received 23 December 2020 • Revised 29 January 2021 • Accepted 1 February 2021*)

Abstract−To investigate the role of vanadium oxide supported on mesoporous silica (VO_x/*m*-SiO_2) catalysts in methane oxidation to formaldehyde, various catalysts were prepared. The type of *m*-SiO_2 (SBA-15 and MCF-17), vanadium loading (1, 3, and 5%), and preparation method (wet impregnation; WI and dry impregnation; DI) were changed to produce VO_x/*m*-SiO_2 with different vanadium species. Because of the larger surface area and pore size, a higher dispersion of vanadium loading, 1% VO_x/MCF-17(DI), showed the highest conversion (20.2%) in methane oxidation at 600 °C. Various characterizations revealed that DI was a better method to produce isolated tetrahedral monovanadate species in VO_x/*m*-SiO_2 catalysts than WI. As the vanadium loading was decreased from 5 to 1%, the methane conversion was further increased due to the higher degree of dispersion of monomeric VO_4 generated in the catalysts with low vanadium loading. The combined results demonstrate that the dispersion of vanadium and the isolated monomeric VO_4 phase increased when the vanadium catalyst was loaded on MCF-17 and prepared by the DI method.

Keywords: Vanadium, Mesoporous Silica, Methane Oxidation, Formaldehyde, Dry Impregnation

INTRODUCTION

Direct oxidation of methane to formaldehyde in a single step is very important in upgrading natural gas to more valuable chemicals. Essentially, the indirect methane catalytic process that converts methane to formaldehyde proceeds via three steps: steam reforming of methane to produce syngas, conversion of syngas to methanol, and partial oxidation of methanol to formaldehyde [1-4]. However, the four symmetrical sigma C-H bonds of methane ($\Delta H_{C\text{-}H}$= 438.8 kJ mol^{-1}) are kinetically inert and, therefore, difficult to engage in catalytic oxidation reactions; hence, high temperature over 500 °C is generally required for methane activation [5,6]. For direct oxidation of methane to formaldehyde, highly dispersed MoO_x and VO_x supported on SiO_2 exhibit higher activity at elevated temperature (550-600 °C). However, the maximum single pass yield of MoO_x and VO_x catalysts supported on SiO_2 is generally reported to be around 2-10% [7-10]. In addition, the metastable formaldehyde may be further oxidized, producing CO_2 and H_2O as undesirable products during the oxidation process at high temperature. Herman et al. compared V_2O_5 and MoO_3 catalysts supported on SiO_2 prepared by the wet impregnation (WI) method, in the partial oxidation of methanol to formaldehyde. The reported activity of V_2O_5/SiO_2 and MoO_3/SiO_2 catalysts was 9.52% and 0.08% with a formaldehyde selectivity of 15.7% and 100% at 630 °C, respectively [11]. Parmaliana et al. reported that VO_x supported on mesoporous silicas (*m*-SiO_2) prepared by the WI method exhibited two orders of magnitude higher reaction rate than that of MoO_3 catalysts, at 600 °C [12]. Due to these harsh conditions and low conversion rates, there are few studies on the direct oxidation of methane to formaldehyde. According to the previous results using V_2O_5/SiO_2 catalysts, it was found that most of the methane to formaldehyde conversion reactions at about 600 °C showed a low conversion of less than 10%. In particular, *m*-SiO_2 with a large surface area has been used as a good support, but more systematic research is needed. Fundamental research aimed at the development and understanding of catalysts with high efficiency should be carried out in consideration of the abundance and future value of methane resources.

Mesoporous materials have been widely used as excellent supports for incorporating active metals or oxides with high dispersion, owing to their high surface area, large pore volume, and well-ordered pore structure [13-16]. Among them, *m*-SiO_2 is preferentially selected because it is produced by simple sol-gel chemistry with high reproducibility. Depending on the micellar structure determined by the concentration and type of surfactants, including alkylammonium salts and block copolymers, a versatile *m*-SiO_2 structure can be formed with controlled pore structure. The resulting high surface area and well-organized internal pores serve to anchor active oxide species, which is advantageous because the degree of dispersion of vanadium oxides is known to be influenced by the surface structure of the support. Depending on the loading of the vanadium precursor and the resulting dispersion, three types of states are formed in the supported vanadium oxide catalysts: an isolated species, a thin polymeric overlayer, and crystalline V_2O_5 [17]. The preparation method also influences the surface structure of the supported vanadium oxide catalysts. It was reported that the molecular structure was strongly affected by the pH of the vanadium precursor solution used during WI synthesis, which is the most popular and general method for the preparation of supported

†To whom correspondence should be addressed.
E-mail: edpark@ajou.ac.kr, kjan@unist.ac.kr

catalysts. The highly dispersed monomeric structure of the vanadium oxide changed to the polymerized form and finally to the V_2O_5 bulk structure as the pH decreased: $[VO_4]^{3-} \rightarrow [V_2O_7]^{2-} \rightarrow [V_4O_{12}]^{4+} \rightarrow [V_{10}O_{27}(OH)]^{5-} \rightarrow V_2O_5$ bulk [18]. When the solvent-free dry impregnation (DI) method was used, more distorted surface species such as $[VO_4]^{3+}$ can be obtained [19].

To determine the best $VO_x/m\text{-}SiO_2$ catalyst with highest catalytic performance in methane oxidation to formaldehyde, we prepared a series of $VO_x/m\text{-}SiO_2$ catalysts by changing the type of $m\text{-}SiO_2$, vanadium loading, and preparation method. Using these catalysts, we investigated how the loading of V on $m\text{-}SiO_2$ with different surface areas and pore structure influences the configuration of the VO_x active species and the corresponding catalytic reaction. Here, we prepared the $VO_x/m\text{-}SiO_2$ catalysts with three different vanadium loadings (1, 3, and 5%) by the WI and DI methods. Two types of $m\text{-}SiO_2$, SBA-15 and MCF-17 were used to investigate the role of $VO_x/m\text{-}SiO_2$ catalysts. Transmission electron microscopy (TEM), Brunauer-Emmett-Teller (BET) measurements, X-ray diffraction (XRD), temperature-programmed reduction with H_2 (H_2-TPR), ultraviolet-visible spectroscopy (UV-Vis), and Raman spectroscopy were used to determine the major species of vanadium oxides depending on the type of $m\text{-}SiO_2$, vanadium loading, and preparation method. The activity and selectivity of the methane oxidation to HCHO were also correlated with the vanadium species.

MATERIALS AND METHODS

1. Preparation of $m\text{-}SiO_2$ (SBA-15 and MCF-17)

Two different mesoporous silicas, SBA-15 and MCF-17, were synthesized by the reported methods with slight modification [20,21]. For the preparation of SBA-15, 37 g of Pluronic P123 ($EO_{20}PO_{70}EO_{20}$; EO=ethylene oxide, PO=propylene oxide, Sigma-Aldrich, average M_w=5,800) as a structure-directing agent were dissolved in 185 mL of concentrated hydrochloric acid (HCl, 35.0-37.0%) and 1.16 L of water in a sealed polypropylene bottle under vigorous stirring at 35 °C for 5 h. Subsequently, 84 mL of tetraethyl orthosilicate (Sigma-Aldrich, 98%) in a separating funnel was added to the solution mixture and kept at 35 °C overnight without stirring. Hydrothermal treatment involved storing the bottle in an oven at 80 °C for 24 h. The resulting white slurry was filtered by a vacuum filter and washed with deionized water and ethanol. After calcination in air at 550 °C for 6 h, SBA-15 in the form of white powder was collected. MCF-17 was synthesized by a similar procedure as that adopted for SBA-15 [22]. In brief, 40 g of Pluronic P123 and 40 g of 1,3,5-trimethylbenzene (Sigma-Aldrich, 98%) were dissolved in 100 mL of concentrated HCl and 650 mL of water under vigorous stirring at 35 °C for 5 h. Then, 92 mL of tetraethyl orthosilicate was added in the same manner and kept at 35 °C overnight. Before the hydrothermal process at 80 °C, 0.46 g of ammonium fluoride (NH_4F, Sigma-Aldrich, 98%) was added as a mineralizer to the solution. Filtration, washing, and calcination were by the same procedure as the SBA-15 synthesis to obtain powdered MCF-17.

2. Fabrication of $VO_x/m\text{-}SiO_2$ Catalysts

Two different preparation methods were used for $VO_x/m\text{-}SiO_2$ catalysts: WI and DI. For the WI, ammonium metavanadate (NH_4VO_3, Alfa Aesar, 99%), vanadyl acetylacetonate ($VO(acac)_2$, Sigma-Aldrich, 97%), and oxalic acid ($H_2C_2O_4$, Acros, 99+%) were used. A certain amount of NH_4VO_3 calculated according to the metal loading was dissolved in water, and then, $H_2C_2O_4$ was added to the solution. The solution was stirred vigorously until the color changed to blue. After the addition of as-synthesized $m\text{-}SiO_2$, the mixed slurry was dried overnight at 100 °C and calcined at 400 °C for 3 h. The resulting catalyst was pelletized and sieved to 150-250 μm particulate size before use in the catalytic reaction. For the DI, $VO(acac)_2$ and $m\text{-}SiO_2$ were mixed according to the metal loading in a mortar. After physical mixing in a mortar, the powder was loaded in a crucible inside a tubular furnace. Thermal treatment in N_2 atmosphere at 240 °C for 3 h and calcination with O_2 were carried out at 500 °C for 17 h for complete oxidation. The obtained catalysts were pelletized and sieved in the same manner of the WI method.

3. Characterization

Nitrogen adsorption isotherms were obtained using a Microtrac BELsorp-max analyzer after outgassing the sample at 150 °C for 12 h. The pore size distribution was determined by the Barrett-Joyner-Halenda (BJH) method. Powder XRD was carried out in the 2θ range of 10-80° (Cu Kα radiation, λ=1.5418 Å) using a PANalytical X'Pert Pro. TEM measurement was performed using a JEOL JEM-2100F instrument operated at 200 kV. H_2-TPR was carried out in a Micromeritics AutoChem II 2920 instrument. In short, a catalyst sample (50 mg) was prepared into a U-shaped quartz tube and outgassed under pure He flow (50 NmL min^{-1}) for 30 min to remove moisture and impurities. After cooling to 50 °C, 10 vol% H_2/He stream (50 NmL min^{-1}) was introduced and the temperature was raised to 800 °C at 10 °C min^{-1} heating rate. The amount of consumed H_2 was recorded by gas chromatography (GC) using a Delsi Nermag thermal conductivity detector (TCD). UV-Vis diffuse reflectance spectra were obtained by an Agilent Cary 5000 UV-Vis-NIR spectrophotometer measured from 200-2,200 nm, and a halon white reflectance standard was used as the standard. Raman analysis was carried out on a WITec alpha300R spectrometer equipped with 532 nm laser excitation. The spectra were collected using a charge-coupled device detector with a 10 s exposure and 10-fold accumulation.

4. Methane Oxidation

Catalytic methane oxidation was carried out under atmospheric pressure and at a constant temperature of 600 °C in a laboratory-scale fixed bed reactor. $VO_x/m\text{-}SiO_2$ catalyst (100 mg) was loaded into a quartz tube (inner diameter=1 cm) together with 1 g of purified quartz sand. A gas mixture of CH_4 and O_2 was fed through the catalyst bed using a mass flow controller (total flow of 40 mL min^{-1}, 24,000 mL g_{cat}^{-1} h^{-1}, 1 : 1 molar ratio). The reaction temperature was detected by a K-type thermocouple closely attached to the inside of the catalyst bed covered by the furnace. The product composition was analyzed using an on-line GC (YL6500) equipped with Porapak-N and molecular sieve columns using Ar as a carrier gas. The separated gases, including H_2, CO_2, CO, and CH_4, were detected by the GC, which was connected to both TCD and flame ionization detector (FID) with a methanizer. No methane conversion was detected when the reaction was measured in an empty quartz reactor or when only $m\text{-}SiO_2$ without vanadium load-

ing was tested. Before entering the GC, HCHO was trapped in a cold trap containing 10.5 g of Na_2SO_3 and 1.63 g of H_2SO_4 dissolved in 100 mL of aqueous solution. The concentration of HCHO was quantitatively determined by titration between the produced NaOH and the contained H_2SO_4 residue [7,23,24].

RESULTS AND DISCUSSION

1. Structural Characterizations of VO_x/m-SiO_2 Catalysts

Two different mesoporous silicas, MCF-17 and SBA-15, were used to load vanadium with a weight percent of 1, 3, and 5. Each VO_x/m-SiO_2 catalyst was prepared by either the WI or DI method. Fig. 1 shows TEM images, XRD patterns, and N_2 adsorption/desorption isotherms of 1, 3, and 5% VO_x/MCF-17 and VO_x/SBA-15 catalysts through the WI method. The TEM images shown in Fig. 1 reveal that the pore size of MCF-17 (30-50 nm) is greater than that of SBA-15 (≤10 nm diameter). Unlike MCF-17 with mesocellular pore structure generated by a pore-swelling agent, 1,3,5-trimethylbenzene, SBA-15 has well-ordered hexagonal channels with a *p6mm* symmetry. However, the vanadium species are hardly distinguishable from the m-SiO_2 in the TEM images due to the high dispersion and small size of the VO_x. Fig. 1(b) shows the XRD patterns measured in the range of 10-80°. The broad reflection at 23° originated from the amorphous m-SiO_2. The characteristic reflections

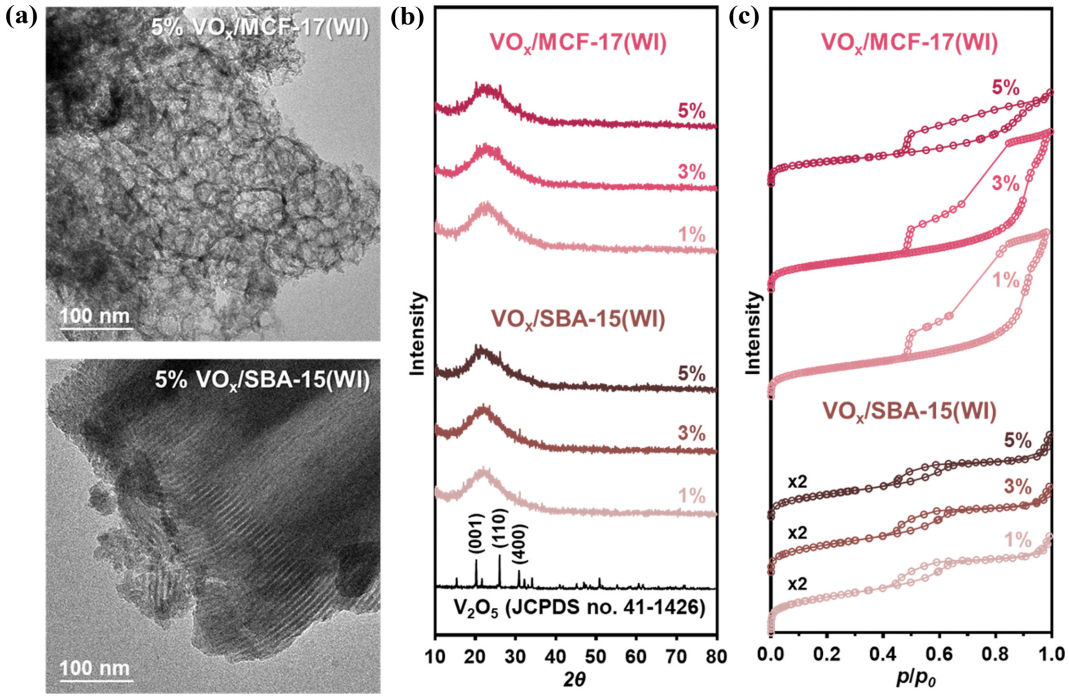

Fig. 1. VO_x/m-SiO_2 catalysts prepared by the wet impregnation (WI) method: (a) TEM images of 5% VO_x/MCF-17 and VO_x/SBA-15, (b) XRD patterns and (c) N_2 adsorption-desorption isotherms of VO_x/m-SiO_2 catalysts with different vanadium loading.

Table 1. BET surface areas (a_s) and pore diameters (d_{pore}) of VO_x/m-SiO_2 catalysts

Catalyst	Vanadium loading	Surface area	Pore diameter
	(%)	a_s, ($m^2\ g^{-1}$)	d_{pore}, (nm)
VO_x/MCF-17 (WI)	1	652	9.00
	3	617	9.12
	5	578	9.24
VO_x/SBA-15 (WI)	1	361	4.61
	3	347	4.58
	5	318	4.80
VO_x/MCF-17 (DI)	1	750	7.13
	3	582	7.86
	5	506	8.36
VO_x/SBA-15 (DI)	1	350	5.46
	3	362	5.50
	5	275	5.44

of V_2O_5 at 20° and 26°, which are assigned to the (001) and (110) phases, appear slightly as the vanadium loading increases. Fig. 1(c) shows the N_2 adsorption-desorption isotherms of the VO_x/MCF-17 and VO_x/SBA-15 catalysts. Surface areas determined by BET measurements and pore diameters calculated by the BJH method are summarized in Table 1. The type IV isotherm trend shown in Fig. 1(c) clearly the demonstrates of mesoporous structures of all VO_x/*m*-SiO_2 catalysts. The catalyst supported on MCF-17 has a larger hysteresis curve area than that of SBA-15, while the surface area of VO_x/MCF-17 (570-700 m^2 g^{-1}) is also greater than that of VO_x/SBA-15 (300-360 m^2 g^{-1}). Fig. 1(c) indicates that the surface area of the catalysts decreases gradually as the vanadium content increases.

Fig. 2 shows characterization results of VO_x/MCF-17 and VO_x/

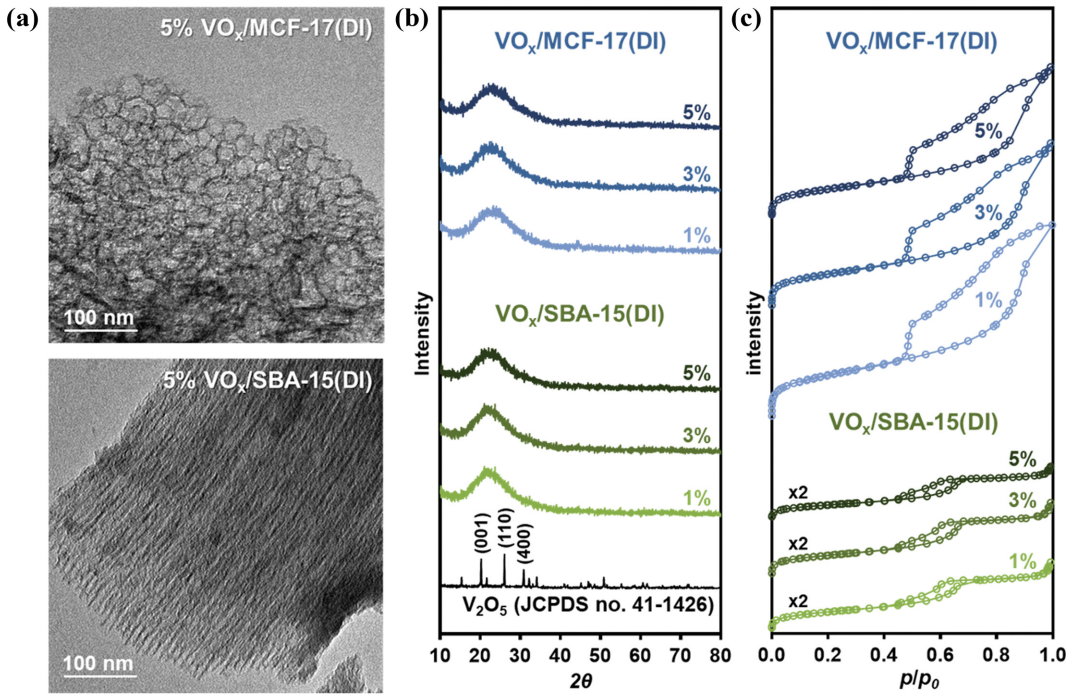

Fig. 2. VO_x/*m*-SiO_2 catalysts prepared by the dry impregnation (DI) method: (a) TEM images of 5% VO_x/MCF-17 and VO_x/SBA-15, (b) XRD patterns and (c) N_2 adsorption-desorption isotherms of VO_x/*m*-SiO_2 catalysts with different vanadium loading.

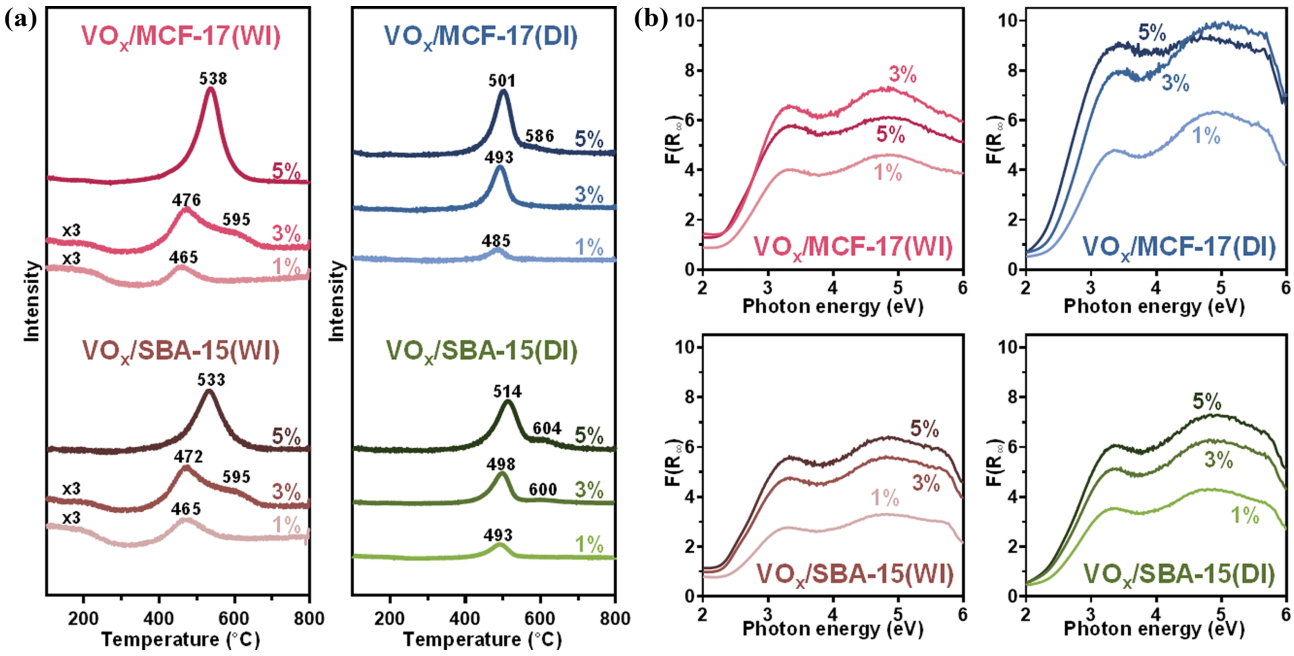

Fig. 3. (a) H_2-TPR and (b) UV-Vis diffuse reflectance spectra of VO_x/*m*-SiO_2 catalysts.

SBA-15 catalysts prepared by the DI method. Again, the TEM images do not clearly identify the VO_x species on the silica support. Similarly, the XRD patterns in Fig. 2(b) show that the VO_x species is hardly detectable due to the high dispersion and small size of the VO_x species. XRD measurements of surface vanadium species are only suitable for bulk structures for nanoparticles of at least 4 nm or larger [25]. For this reason, the crystal structure of the VO_x cannot be identified clearly by the current characterization tools. Surface areas and pore diameters of VO_x/MCF-17 and VO_x/SBA-15 catalysts prepared by the DI method have similar results to those of the WI method (Fig. 2(c) and Table 1). The surface areas of MCF-17 catalysts are evaluated to be about twice higher than that of SBA-15 catalysts due to the structural difference of the mesoporous silicas. The structure of MCF-17 has larger pores with the undulations of mesopores by addition of trimethylbenzene, whereas SBA-15 has narrow size distribution (Fig. S1). HAADF-STEM and EDS mapping images of 5% VO_x/SBA-15(WI) and 5% VO_x/MCF-17(DI) showed high dispersion of vanadium on both *m*-SiO_2 regardless of the preparation method of catalysts (Fig. S2). From these results, it is revealed that both WI and DI methods produced VO_x/*m*-SiO_2 catalysts with a high dispersion of vanadium species on *m*-SiO_2 supports and the preparation method does not affect the physical properties of the catalyst.

2. Active Vanadium Phases of VO_x/*m*-SiO_2 Catalysts

The concentration of the VO_x species on *m*-SiO_2 supports is highly correlated with the nature of the vanadium active sites, which contain the terminal V=O group as an isolated tetrahedral monovanadate (VO_4) species [26]. The structure of the supported VO_x species can be changed on metal oxides (SiO_2, ZrO_2, Al_2O_3, and TiO_2) with various chemical properties, due to surface interactions at high temperature [27]. The chemical information of the VO_x active species, including reducibility, distribution, and quantity, was identified by H_2-TPR spectra. Fig. 3(a) shows TPR profiles of VO_x/*m*-SiO_2 catalysts obtained at 100-800 °C. Below 500 °C, a representative peak is observed of the isolated V^{5+} species in $[VO_4]^{3-}$ on the *m*-SiO_2 support. This represents a vanadium species in the form of a distorted tetrahedral coordination site with one short V=O and three V-O bonds attached to the support [9,28]. Crystalline V_2O_5 species appear at higher reduction temperatures [2,29]. As the vanadium loading increases in the VO_x/*m*-SiO_2 catalysts, the main peak shifts to higher temperature and the peak intensity increases. The H_2-TPR spectra of the 3% VO_x/SBA-15 and VO_x/MCF-17 catalysts prepared by the WI method show shoulder peaks at 595 °C, indicating crystalline V_2O_5, while the same catalysts with 5% loading have higher peak intensity at 533-538 °C corresponding to the polymeric and crystalline V_2O_5 phase (Fig. 3(a), left). The 5% loaded VO_x/SBA-15 and VO_x/MCF-17 catalysts prepared by the DI method have major peaks at 501 and 514 °C, respectively. They also have a minor shoulder peaks at 586 and 604 °C, demonstrating that they still have dominant isolated $[VO_4]^{3-}$ species, compared to the overlapped peaks derived from the isolated and crystalline phase of 5% VO_x/*m*-SiO_2 catalysts prepared by the WI method (Fig. 3(a), right). It was revealed that the DI method is much more efficient in creating monomeric VO_4 species in VO_x/*m*-SiO_2 catalysts.

Diffuse reflectance UV-Vis spectra of VO_x/*m*-SiO_2 catalysts were obtained in the range of 2-6 eV (620-210 nm). The square root of the Kubelka-Munk function multiplied by the photon energy $(F(R_\infty)hv)^{1/2}$ versus the photon energy (hv) was plotted to determine the dispersion and local structure of VO_x on the support (Fig. 3(b))[30-32]. The value of the absorption energy band (ε_0) was calculated by extrapolation of the Kubelka-Munk function from the linear fit of the *x*-intercept at the low-energy side. The ε_0 value of more than 3 eV is assigned to the presence of VO_x species with T_d coordination, whereas a value lower than 3 eV is ascribed to polymeric or further bulk V_2O_5. There is no obvious change in the ε_0 values (2.11-2.35 eV) of the V_2O_5/*m*-SiO_2 catalysts as a function of vanadium loading, indicating that they possess a dominant V_2O_5 phase. However, V_2O_5/MCF-17(DI) catalysts with 1, 3, and 5% of vanadium loading have 2.35, 2.32, and 2.11 eV ε_0 value, respectively. In particular, 1% VO_x/MCF-17(DI) showed the highest ε_0 value (2.35 eV), demonstrating the highest amount of monomeric VO_x species on *m*-SiO_2. These results demonstrated that V_2O_5/*m*-SiO_2 catalysts prepared by the DI method show higher ε_0 values due to more numerous monomeric T_d species than those of catalysts by the WI method.

Raman spectroscopy was also used to identify an active vanadium site, including monomeric and polymeric vanadyl species [33-35]. Fig. 4 shows the Raman spectra of VO_x/*m*-SiO_2 catalysts depending on the synthesis method and vanadium loading. The peak at 1,040 cm^{-1} indicates the V=O stretching from monomeric VO_4 species, and the peaks at 140, 285, 305, 406, 521, 703, and 995 cm^{-1} correspond to the presence of crystalline V_2O_5 phase originating from a second V=O Raman stretching [36]. In Fig. 4(a), the monomeric VO_4 phase is dominant in 1% V_2O_5/*m*-SiO_2 catalysts prepared by the WI method. As the vanadium content increases to 3 and 5%, the monomeric phase disappears and a distinct V_2O_5 peak appears at 995 cm^{-1} (Fig. 4(a)). VO_x/SBA-15(DI) catalysts have a similar peak at 995 cm^{-1} (Fig. 4(b)), because of the crystalline V_2O_5 phase. However, VO_x/MCF-17(DI) catalysts with a higher surface

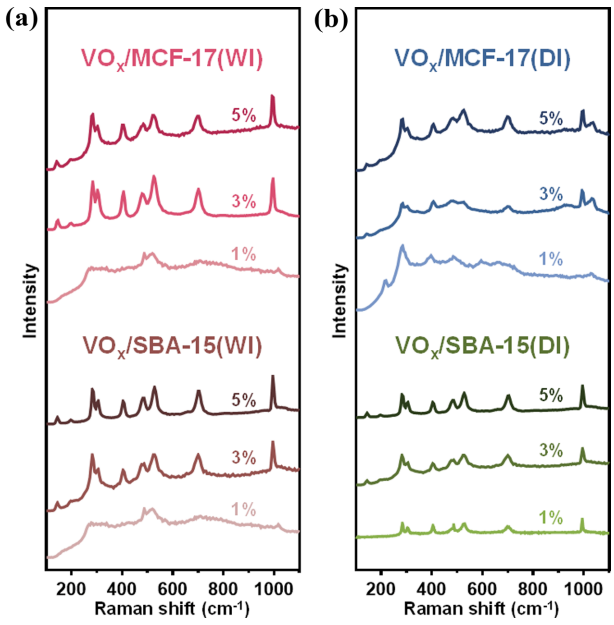

Fig. 4. (a) Raman spectra of VO_x/*m*-SiO_2 catalysts prepared by (a) WI and (b) DI methods.

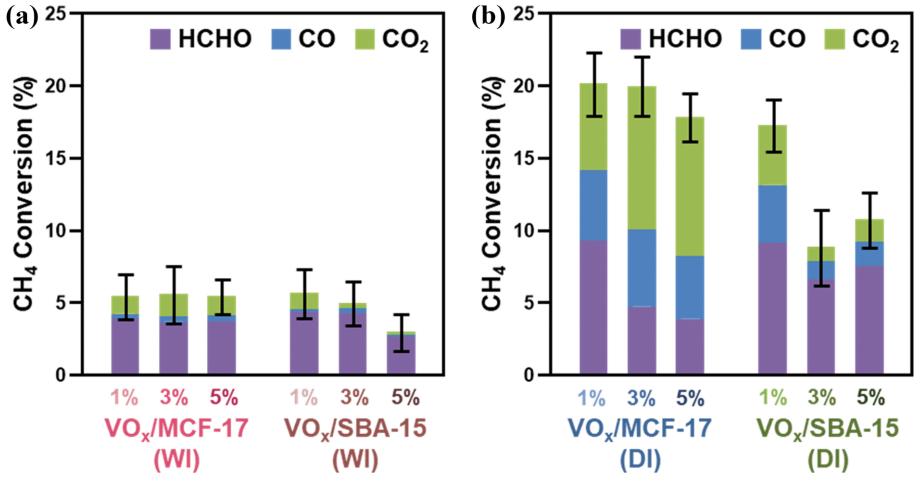

Fig. 5. (a) Catalyst results of methane oxidation to formaldehyde over VO_x/m-SiO_2 catalysts prepared by (a) WI and (b) DI methods. Reaction conditions: CH_4/O_2 volume ratio of 1 : 1, 600 °C, 1 bar, W_{cat}=100 mg, GHSV=24,000 mL g_{cat}^{-1} h^{-1}.

area show distinct peaks at 1,040 cm^{-1}, revealing the presence of VO_4 species regardless of the vanadium content. The overall Raman peaks are sharper for the VO_x/m-SiO_2(WI) due to higher content of the crystalline V_2O_5 than for VO_x/m-SiO_2(DI). Although VO_x/MCF-17(DI) catalysts also have the crystalline V_2O_5 phase, they contain the monomeric VO_4 phase as well. Depending on the synthesis method, the distribution of the surface vanadium species is different in VO_x/m-SiO_2 catalysts.

3. Methane Oxidation to Formaldehyde

Catalytic methane oxidation was carried out in a fixed bed reactor at 600 °C in the presence of various VO_x/m-SiO_2 catalysts. Fig. 5 and Table S1 summarize the catalytic results, including the methane conversion and the HCHO selectivity. Methane conversion is determined from the results of three repeated reactions and the deviations are indicated by error bars. While all VO_x/m-SiO_2(WI) catalysts show low methane conversion, less than 6% (Fig. 5(a)), VO_x/m-SiO_2(DI) of the catalysts exhibit much higher conversion than VO_x/m-SiO_2(WI). In particular, VO_x supported on MCF-17 show higher conversion percentages than those of SBA-15 prepared by DI, demonstrating that MCF-17 with its higher surface area and distinct mesocellular pore structure is a better support than SBA-15. As the vanadium content decreases to 1%, the methane conversion increases, demonstrating that a high dispersion of VO_x is crucial for methane oxidation to formaldehyde. Among the catalysts, 1% VO_x/MCF-17(DI) shows the highest conversion (20.2%) because of the distinct monomeric VO_4 phase (Fig. 5(a)). As the CH_4 conversion increases, a general trend of decrease in HCHO selectivity due to deep oxidation was observed. The high methane conversion of VO_x/MCF-17(DI) catalysts also yields greater selectivity for CO_2. However, the calculated production of net formaldehyde was much higher in VO_x/MCF-17(DI) catalysts with the high methane conversion. The Raman spectroscopy in Fig. 4 shows a clear V=O bond stretch from the isolated species in all VO_x/MCF-17(DI) catalysts that recorded high CH_4 conversion regardless of the vanadium loading. In addition, the results of H_2-TPR showed a small change in peak maxima with vanadium loading, indicating a consistent monomeric VO_4 species in MCF-17. Also, the smallest ε_0 value of 1% VO_x/MCF-17(DI) represents the monomeric VO_4 species. Therefore, the vanadium content of VO_x/m-SiO_2 catalysts correlated with methane conversion clearly demonstrates that the dispersion of vanadium and the monomeric VO_x phase are the most important factors for methane oxidation to formaldehyde. The DI method was also shown to be a better synthesis method than the WI for high distribution of isolated tetrahedral species on m-SiO_2. In general, it is easy to think that using a solvent will make it more homogeneous, but it seems to be limited to a macroscopic point of view. When impregnation is carried out using a solvent (WI), the uniformity is often poor during the drying process [37]. A rotary evaporator is used to make the catalyst as uniform as possible for preparation. However, the WI causes a wide distribution of active species as the dissolved vanadium precursor solution forms water droplets on the catalyst surface during drying. As the solvent evaporates, the concentration imbalance is tilted towards the edge of the droplet rather than the center [38]. This leads to a mixture of monomeric VO_4 species and bulk structure despite the low vanadium loading in the calcination process, and most of the vanadium load can be agglomerated. On the other hand, in the DI method, heat treatment proceeds immediately after solid mixing. Except for molecular transport through the calcination process, the aggregation of vanadium has limitations. Therefore, high dispersion catalysts can be synthesized by DI method rather than WI.

CONCLUSIONS

The isolated monomeric VO_4 species proved to be a key active species for methane oxidation to formaldehyde. This is evidenced on the basis of the reaction results and properties of the catalyst prepared by three factors. The role of VO_x/m-SiO_2 catalysts was investigated by varying the type of m-SiO_2 (SBA-15 and MCF-17), vanadium loading (1%, 3%, and 5%), and preparation method (WI and DI). Because the surface area and pore size of MCF-17 were greater than that of SBA-15, the VO_x/MCF-17 catalysts resulted in higher dispersion of the vanadium species. H_2-TPR and Raman

results showed that DI was the better method for obtaining the isolated tetrahedral monovanadate species in VO_x/m-SiO_2 catalysts. Methane oxidation over various VO_x/m-SiO_2 catalysts at 600 °C showed that VO_x/m-SiO_2(DI) catalysts led to much higher conversion rates than VO_x/m-SiO_2(WI). As the vanadium content was decreased to 1%, the methane conversion increased, because of the high dispersion of monomeric VO_4 in the catalysts with low vanadium loading. Owing to the high surface area and distinct mesocellular pore structure of MCF-17, 1% VO_x/MCF-17(DI) showed the highest conversion (20.2%). As the methane conversion increased, the selectivity toward formaldehyde decreased; however, the net production of formaldehyde was much higher when using VO_x/MCF-17(DI) than when using the VO_x/SBA-15(DI) and VO_x/SBA-15(WI) catalysts. In particular, VO_x/m-SiO_2 prepared by using MCF-17 via the DI method was proven to be the best catalyst for the direct conversion of methane oxidation to formaldehyde.

ACKNOWLEDGEMENTS

This research was supported by C1 Gas Refinery Program through the National Research Foundation of Korea (NRF) funded by the Ministry of Science, ICT & Future Planning (2015M3D3A1A01 064899), and by Technology Innovation Program funded by the Ministry of Trade, Industry & Energy (MOTIE, 20010853).

SUPPORTING INFORMATION

Additional information as noted in the text. This information is available via the Internet at http://www.springer.com/chemistry/journal/11814.

REFERENCES

1. N. Ohler and A. T. Bell, *J. Catal.*, **231**, 115 (2005).
2. F. Arena, N. Giordano and A. Parmaliana, *J. Catal.*, **167**, 66 (1997).
3. N. Ohler and A. T. Bell, *J. Phys. Chem. B*, **110**, 2700 (2006).
4. J. H. Lunsford, *Catal. Today*, **63**, 165 (2000).
5. C. Hammond, S. Conrad and I. Hermans, *ChemSusChem*, **5**, 1668 (2012).
6. M. Monai, T. Montini, R. J. Gorte and P. Fornasiero, *Eur. J. Inorg. Chem.*, **25**, 2884 (2018).
7. L. Nguyen, S. Loridant, H. Launay, A. Pigamo, J. Dubois and J. Millet, *J. Catal.*, **237**, 38 (2006).
8. F. Arena and A. Parmaliana, *Acc. Chem. Res.*, **36**, 867 (2003).
9. G. Du, S. Lim, Y. Yang, C. Wang, L. Pfefferle and G. L. Haller, *Appl. Catal. A: Gen.*, **302**, 48 (2006).
10. G. J. Hutchings, M. S. Scurrell and J. R. Woodhouse, *Chem. Soc. Rev.*, **18**, 251 (1989).
11. R. G. Herman, Q. Sun, C. Shi, K. Klier, C.-B. Wang, H. Hu, I. E. Wachs and M. M. Bhasin, *Catal. Today*, **37**, 1 (1997).
12. A. Parmaliana, V. Sokolovskii, D. Miceli, F. Arena and N. Giordano, *ACS Symp. Ser., Am. Chem. Soc.,* Washington, DC, 43 (1993).
13. X. H. Sun, Y. F. Shi, P. Zhang, C. M. Zheng, X. Y. Zheng, F. Zhang, Y. C. Zhang, N. J. Guan, D. Y. Zhao and G. D. Stucky, *J. Am. Chem. Soc.*, **133**, 14542 (2011).
14. C. Perego and R. Millini, *Chem. Soc. Rev.*, **42**, 3956 (2013).
15. D. Gu and F. Schuth, *Chem. Soc. Rev.*, **43**, 313 (2014).
16. P. Wallis, S. Wohlrab, V. N. Kalevaru, M. Frank and A. Martin, *Catal. Today*, **278**, 120 (2016).
17. K. Inumaru, M. Misono and T. Okuhara, *Appl. Catal. A: Gen.*, **149**, 133 (1997).
18. I. E. Wachs, *Dalton Trans.*, **42**, 11762 (2013).
19. J. A. Schwarz, C. Contescu and A. Contescu, *Chem. Rev.*, **95**, 477 (1995).
20. D. Zhao, J. Sun, Q. Li and G. D. Stucky, *Chem. Mater.*, **12**, 275 (2000).
21. T. Klimova, A. Esquivel, J. Reyes, M. Rubio, X. Bokhimi and J. Aracil, *Micropor. Mesopor. Mater.*, **93**, 331 (2006).
22. C.-K. Tsung, J. N. Kuhn, W. Huang, C. Aliaga, L.-I. Hung, G. A. Somorjai and P. Yang, *J. Am. Chem. Soc.*, **131**, 5816 (2009).
23. S. Siggia and W. Maxcy, *Anal. Chem.*, **19**, 1023 (1947).
24. T. Sugino, A. Kido, N. Azuma, A. Ueno and Y. Udagawa, *J. Catal.*, **190**, 118 (2000).
25. C. A. Carrero, R. Schloegl, I. E. Wachs and R. Schomaecker, *ACS Catal.*, **4**, 3357 (2014).
26. G. Du, S. Lim, M. Pinault, C. Wang, F. Fang, L. Pfefferle and G. L. Haller, *J. Catal.*, **253**, 74 (2008).
27. B. Olthof, A. Khodakov, A. T. Bell and E. Iglesia, *J. Phys. Chem. B*, **104**, 1516 (2000).
28. D. Wei, H. Wang, X. Feng, W.-T. Chueh, P. Ravikovitch, M. Lyubovsky, C. Li, T. Takeguchi and G. L. Haller, *J. Phys. Chem. B*, **103**, 2113 (1999).
29. V. Sokolovskii, F. Arena, S. Coluccia and A. Parmaliana, *J. Catal.*, **173**, 238 (1998).
30. X. Gao and I. E. Wachs, *J. Phys. Chem. B*, **104**, 1261 (2000).
31. L. J. Burcham, G. Deo, X. Gao and I. E. Wachs, *Top. Catal.*, **11**, 85 (2000).
32. X. Gao, S. R. Bare, B. M. Weckhuysen and I. E. Wachs, *J. Phys. Chem. B*, **102**, 10842 (1998).
33. H. Launay, S. Loridant, A. Pigamo, J. Dubois and J. Millet, *J. Catal.*, **246**, 390 (2007).
34. D. E. Keller, T. Visser, F. Soulimani, D. C. Koningsberger and B. M. Weckhuysen, *Vib. Spectrosc.*, **43**, 140 (2007).
35. B. M. Weckhuysen and D. E. Keller, *Catal. Today*, **78**, 25 (2003).
36. A. G. Anshits, E. V. Kondratenko, E. N. Voskresenskaya, L. I. Kurteeva and N. I. Pavlenko, *Catal. Today*, **46**, 211 (1998).
37. R. D. Deegan, O. Bakajin, T. F. Dupont, G. Huber, S. R. Nagel and T. A. Witten, *Nature*, **389**, 827 (1997).
38. S. Kumar, J. S. Katz and C. M. Schroeder, *Phys. Rev. Fluids*, **2**, 114304 (2017).

Supporting Information

Methane oxidation to formaldehyde over vanadium oxide supported on various mesoporous silicas

Euiseob Yang*, Jun Gyeong Lee*, Eun Duck Park,†, and Kwangjin An*,†**

*School of Energy and Chemical Engineering, Ulsan National Institute of Science and Technology (UNIST), Ulsan 44919, Korea
**Department of Chemical Engineering and Department of Energy Systems Research, Ajou University, Suwon 16499, Korea
(*Received 23 December 2020 • Revised 29 January 2021 • Accepted 1 February 2021*)

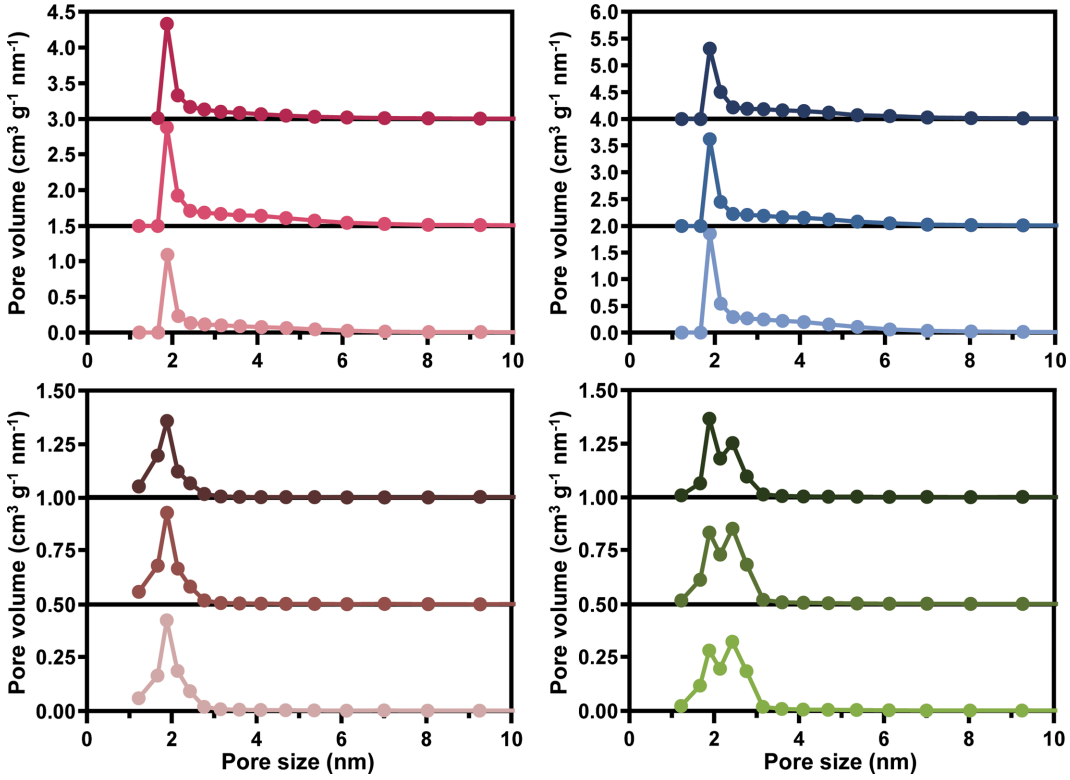

Fig. S1. Pore size distributions of VO_x/*m*-SiO_2 catalysts according to the BJH method.

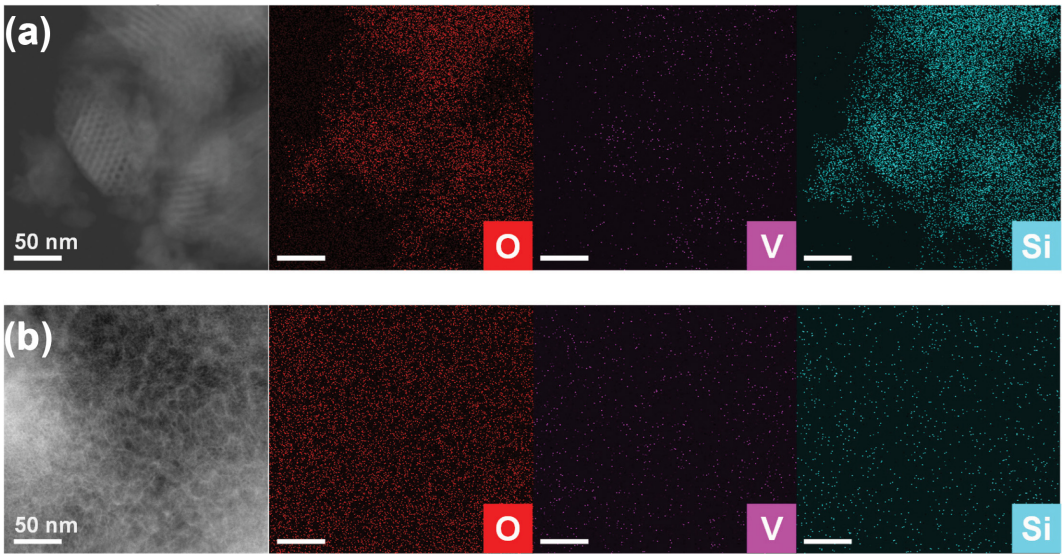

Fig. S2. HAADF-STEM and EDS mapping images of (a) 5% VO_x/SBA-15(WI) and (b) 5% VO_x/MCF-17(DI).

Table S1. Catalyst performance of VO_x/*m*-SiO_2 catalysts in the reaction conditions of CH_4/O_2 volume ratio 1 : 1, 600 °C, 1 bar, W_{cat}=100 mg, GHSV=24,000 mL g_{cat}^{-1} h^{-1}

Catalyst	Vanadium loading (%)	Conversion (%)	Selectivity (%)		
			HCHO	CO	CO_2
VO_x/MCF-17 (WI)	1	5.5	71.2	6.1	22.7
	3	5.6	65.6	7.0	27.4
	5	5.5	67.4	7.5	25.1
VO_x/SBA-15 (WI)	1	5.7	77.0	3.4	19.6
	3	5.0	85.1	7.1	7.9
	5	3.0	89.4	3.4	7.2
VO_x/MCF-17 (DI)	1	20.2	46.1	24.1	29.8
	3	20.0	23.7	26.8	49.5
	5	17.9	21.7	24.3	54.0
VO_x/SBA-15 (DI)	1	17.3	52.9	23.1	24.1
	3	8.9	74.7	13.9	11.3
	5	10.8	69.8	15.9	14.2